The role of miniaturisation in the evolution of the mammalian jaw and middle ear

Stephan Lautenschlager[1,2 *], Pamela Gill[1,3], Zhe-Xi Luo[4], Michael J. Fagan[5], Emily J. Rayfield[1*]

[1]School of Earth Sciences, University of Bristol, UK

[2]School of Geography, Earth and Environmental Sciences, University of Birmingham, UK

[3]Earth Science Department, The Natural History Museum, London, UK

[4]Department of Organismal Biology and Anatomy, University of Chicago, USA

[5]School of Engineering and Computer Science, University of Hull, UK

*Corresponding authors: s.lautenschlager@bham.ac.uk, e.rayfield@bristol.ac.uk

The evolution of the mammalian jaw is one of the most important innovations in vertebrate history, underpinning the exceptional radiation and diversification of mammals over the last 220 million years[1,2]. In particular the mandible's transformation to a single tooth-bearing bone and the emergence of a novel jaw joint while incorporating some of the ancestral jaw bones into the mammalian middle ear is often cited as a classic textbook example for the repurposing of morphological structures[3,4]. Although remarkably well documented in the fossil record, the evolution of the mammalian jaw still poses an intriguing paradox: how could bones of the ancestral jaw joint function both as a joint hinge for powerful load bearing mastication and also as mandibular middle ear that would be delicate enough for hearing? Here, we use new digital reconstructions, computational modelling, and biomechanical analyses to demonstrate that miniaturisation of the early mammalian jaw was the primary driver

for the transformation of the jaw joint. We show that there is no evidence for a concurrent reduction in jaw joint stress and a simultaneous increase in bite force in key non-mammaliaform taxa in the cynodont-mammaliaform transition as previously thought[5-8]. Although a shift in the recruitment of the jaw musculature occurred during the evolution to modern mammals, the optimisation of the mandibular function to increase bite force while reducing joint loads did not occur until after the emergence of the neomorphic mammalian jaw joint. This suggests that miniaturisation provided a selective regime for the evolution of the mammalian jaw joint, followed by the integration of the postdentary bones into the mammalian middle ear.

The mammalian jaw and jaw joint are unique among vertebrates[6]. While the craniomandibular jaw joint (CMJ) of non-mammalian vertebrates is formed between the quadrate and articular bones, mammals evolved a novel jaw hinge between the squamosal and dentary bones (secondary/temporomandibular jaw joint, TMJ)[1-4]. The evolutionary origins of this morphological transformation involved a suite of osteological modifications to the feeding and auditory systems, occurring over a period of 100 million years during the Late Triassic and Jurassic across the cynodont-mammaliaform transition[9,10]. The tooth-bearing dentary bone increased in size relative to the postdentary elements, eventually transforming the seven-bone lower jaw in pre-mammalian cynodonts (referred to as cynodonts hereafter) to a single-bone jaw in modern mammals; parallel to this simplification of the mandible, the integration of elements of the ancestral CMJ into the ossicular chain led to a unique middle and inner ear morphology capable of more sensitive sound detection[11,12]. While new fossil information has suggested that a definitive mammalian middle ear (DMME) evolved independently in at least three mammalian lineages by detachment from the mandible, the emergence of a secondary jaw joint is a key innovation uniting all mammaliaforms[9,13]. However, a central question exists as to how the jaw hinge remained to

be robust enough to bear strong mastication forces, while the same bones in the jaw would become delicate enough to be biomechanically viable for hearing, during this transformation[3,5,10].

The stepwise acquisition of morphological features leading to the emergence of the TMJ is exceptionally well documented in the fossil record by a series of transitional taxa illuminating the evolutionary dynamics involved[4]. Whilst still appearing to function as a jaw joint and viable for sound transmission in cynodonts (e.g. *Thrinaxodon liorhinus*, *Probainognathus*, *Probelesodon sanjuanensis*), the postdentary bones gradually reduced in size and shifted away from the jaw joint – likely for more sensitive hearing[10,12]. This trend resulted in all basal mammaliaforms (e.g. *Sinoconodon rigneyi*, *Morganucodon oehleri*) possessing a remarkable 'dual jaw joint' with two seemingly functional joints: a quadrate-articular joint medial to a mammalian dentary condyle and squamosal glenoid hinge[11,13]. More derived groups and crown mammals eventually lost the ancestral quadrate-articular joint. In addition to fossil evidence, this sequence of events was identified historically in embryonic stages of living mammals[14,15] and recent morphogenetic studies, gene patterning and regulatory networks have elucidated the development of these structures further[16,17]. Previous studies have theorised that muscle reorganisation reduced load at the jaw joint[6,10], yet these claims have not been tested in fossil taxa and experimental studies of extant mammals reveal that the jaw joint usually experiences net compressive loading[18,19]. The modification of the mandible and the emergence of a novel jaw joint and middle ear, therefore, represents an intriguing problem. This is especially puzzling when all the evidence points towards modifications for increased jaw muscle force, consolidation of cranial bones, increased complexity of sutures and supposedly stronger skulls during mammalian evolution[1,5].

Here, we have integrated a suite of digital reconstruction, visualisation and quantitative biomechanical modelling techniques to test the hypothesis that reorganisation of the adductor musculature and reduced stress susceptibility in the ancestral jaw joint facilitated the emergence of the mammalian TMJ. Applying finite element analysis (FEA), we calculated bone stress, strain and deformation to determine the biomechanical behaviour of the mandibles of six key taxa across the cynodont-mammaliaform transition (Fig 1). These analyses were supplemented by multibody dynamics analysis (MDA) to predict bite forces and joint reaction forces. Results from the combined analyses demonstrate that during simulated biting there is no evidence for the reduction of stresses (von Mises, tensile, compressive) in the jaw joint (CMJ and/or TMJ) across the studied cynodont and mammaliaform taxa (Figs. 2, 3, Extended data figs. 1, 3). This was found for unilateral and bilateral biting simulations and regardless of the working and balancing side joint. However, bite position appears to have a moderate effect on joint stresses (particularly compression), with stress increasing as the bite point moves anteriorly along the tooth row. This is consistent with experimental data for extant mammals, in which incisor biting resulted in the highest joint loads[20]. Similarly, MDA results show that absolute joint reaction forces are not reduced while the jaw joint underwent morphological transformation (Figs. 2, 3), whereas relative bite forces (ratio between muscle force and bite force) are found to decrease in derived cynodonts (*Probainognathus* and crownwards) and to stay largely constant in mammaliaforms, such as *Morganucodon oehleri* and *Hadrocodium wui* (Extended data figs 1-3). However, the simulation of different muscle activation patterns using FEA reveals that there is, across the cynodont-mammaliaform transition, a distinct shift in the recruitment of jaw adductor musculature required to achieve high bite forces that maintain low stress in the jaw joint (Fig. 4a). The highest bite forces while keeping joint tensile stresses low are found for jaw adduction dominated by the masseter muscle group in the cynodonts *Thrinaxodon*

liorhinus, *Diademodon tetragonus* and *Probainognathus* sp. In *Probelesodon sanjuanensis* and the mammaliaforms *Morganucodon oehleri* and *Hadrocodium wui* the recruitment of the pterygoideus muscle group (with contribution of the masseter musculature) provides the highest relative bite forces, eventually shifting to the temporalis group as the dominant contributor for high bite force/low joint stress performance in the extant taxon *Monodelphis domestica*. This pattern is reversed for muscle activations optimised for high bite force in relation to low compressive stresses in the jaw joint in mammaliaforms in comparison to cynodonts (Fig. 4a). While this is achieved mainly by recruitment of the temporalis group in cynodonts, the masseter and the pterygoideus groups form the dominant musculature in mammaliaforms. Apart from an overall shift in the pattern of muscle recruitment, the analyses further demonstrate that while in the cynodonts and mammaliaforms a single muscle group is harnessed to achieve 'optimal' bite forces (i.e. high bite force/low jaw joint stress), *Monodelphis domestica* simultaneously activates all three muscles groups (Extended data figs. 4-9) as revealed by the computational analyses here, confirming previous experimental data[21]. Changes to muscle orientation and inferred muscle lines of action either precede or are associated with mandible shape change[22], leading to a more efficient use of the adductor system to maximise bite force and minimise loads on the jaw joint.

Considering that the shape of the mandible alone does not appear to have a substantial influence on stress reduction in the mandibles of the studied taxa, we further tested size-related effects on the biomechanical behaviour of the jaw joint. All taxa were scaled to seven different jaw lengths (5-320 mm) covering the mandibular size range observed across the cynodont-mammaliaform transition (Fig. 1, Fig. 4b, supplementary table S1). Results for these hypothetical resized models demonstrate that absolute tensile and compressive stresses in the jaw joint decrease exponentially to 25% with a reduction in size by 50%. At the same time, absolute bite forces decrease by 50%, in direct proportion to jaw length.

We offer new biomechanical evidence that stress susceptibility of the mandible, and in particular of the jaw joint, was not reduced across the cynodont-mammaliaform transition. This contrasts with existing hypotheses that argue for a reduction of joint loads due to the rearrangement of the jaw adductor musculature and the resultant increase in bite force in mammaliaforms[1,7,8]. The decrease in size of the postdentary bones and the accompanying expansion of bony angular and coronoid projections of the dentary is assumed to have paralleled the reorganisation and evolution of mammalian muscle groups (masseter and temporalis)[6,8,21]. Arranged in such a manner, the changed line of action of the major jaw adductor muscles was hypothesised to have led to a redistribution of muscle forces with little or no load experienced at the jaw hinge. However, our results do not support these previous inferences.

As demonstrated here, a change in the recruitment of the jaw adductor musculature can be observed to achieve high bite forces, while at the same time keeping tensile and compressive joint stresses at a minimum. These findings parallel experimental data from extant mammals that differential muscle activation produces different stress regimes in the jaw joint[20]. However, in the studied cynodonts and mammaliaforms, parallel activation of all three adductor muscle groups does not lead to the highest relative bite forces (Extended data figs. 4-9) as found in *Monodelphis domestica*. Although the mammal-like muscle division and arrangement of the jaw adductors preceded the osteological transformation of the mandible and jaw joint[21], it was not until a later stage in mammalian evolution that further optimisations to muscle function occurred. A recent study[23] using free-body analysis of the cynodont lower jaw confirmed that the musculoskeletal system was morphologically and evolutionary flexible without negatively impacting functional performance.

Rather than alterations of the osteology and the muscular arrangement, reduction in mandibular size produced the most notable effects on minimising absolute jaw joint stress in

our analyses. Although a decrease in size leads to two conflicting trends of reducing tensile and compressive stresses but also bite forces, stress reduction is achieved at a higher rate than bite force reduction (exponential vs linear). Consequently, our biomechanical analyses predict that smaller mandibular size constitutes the best compromise to ameliorate loss of bite force and stress reduction in the jaw joint. This prediction is corroborated by the reduction in size in the vast majority of taxa phylogenetically intermediate in the cynodont-mammaliaform transition, in which such a biomechanical compromise was achieved (Fig. 1, 4b). Miniaturisation has been discussed as a key factor during the evolution of mammals in the context of thermoregulation, nocturnality and dietary/ecological adaptations[1,2,24,25]. It has further been proposed to be a structural requirement for the acquisition of mammalian characters[1]. While size-related stress reduction might not have been the main target for selection, it could have constituted a by-product of adaptation to a specific ecological niche demanding small body size[26] during early phases of radiation[4,27]. Our results demonstrate that changes to joint morphology and muscle (re-)organisation have little impact on joint loading. Instead, reduction in size appears to be key, by lowering stress and strain disproportionately to bite force magnitude. Miniaturisation of the mandibular system could, therefore, be a crossing of an evolutionary Rubicon, in the emergency of the TMJ, and in further functional integration of postdentary bones in the middle ear, before their final separations from the mandible in respective lineages, leading to a spectacular diversification of crown mammals.

1. Kemp, T. S. *The Origin and Evolution of Mammals* (Oxford Univ. Press, Oxford, 2005).
2. Kielan-Jaworowska, Z. et al. *Mammals from the Age of Dinosaurs—Origins, Evolution, and Structure* (Columbia Univ. Press, New York, 2004).

3. Crompton, A. W. Evolution of the jaw articulation in cynodonts *in* Joysey, K. A. & Kemp, T. S. *Studies in Vertebrate Evolution*. (Oliver & Boyd, Edinburgh, 1972), 231-253.
4. Luo, Z.-X. Transformation and diversification in early mammal evolution. *Nature*. **450**, 1011–1019 (2007).
5. Crompton, A.W., Hylander, W. L. Changes in mandibular function following the acquisition of a dentary-squamosal joint. *in The Ecology and Biology of Mammal-like Reptiles* (eds N. Hotton III, P. D. MacLean, J. J. Roth, E. C. Roth, Smithsonian Institution Press, Washington.), 263-282 (1986).
6. Bramble, D. M. Origin of the mammalian feeding complex: models and mechanisms. *Paleobiology* **4**, 271-301 (1978).
7. Barghusen, H. R. in *Morphology of the maxillomandibular apparatus* (ed G. H. Schumacher) 26-32 (VEB Georg Thieme, 1972).
8. DeMar, R. & Barghusen, H. R. Mechanics and the evolution of the synapsid jaw. *Evolution* **26**, 622-637 (1972).
9. Luo, Z.-X. Developmental patterns in Mesozoic evolution of mammal ears. *Ann. Rev. Ecol. Evol. Syst.* **42**, 355-380 (2011).
10. Allin, E. F. Evolution of the mammalian middle ear. *J. Morph.* **147**, 403-437 (1975).
11. Sidor, C. A. Evolutionary trends and the origin of the mammalian lower jaw. *Paleobiology* **29**, 605-640 (2003).
12. Manley, G. A. Evolutionary paths to mammalian cochleae. *J. Assoc. Res. Otolaryngology* **13**, 733-743 (2012).
13. Luo, Z.-X., et al. New evidence for mammaliaform ear evolution and feeding adaptation in a Jurassic ecosystem. *Nature* **548,** 326 (2017).

14. Reichert, C. Über die Visceralbogen der Wirbelthiere im Allgemeinen und deren Metamorphosen bei den Vögeln und Säugethieren. *Archiv für Anatomie, Physiologie und wissenschaftliche Medicin*, 120-222 (1837).
15. Gaupp, E. W. T. Die Reichertsche Theorie (Hammer-, Amboss und Kieferfrage). *Archiv für Anatomie und Entwicklungsgeschichte* **1912**, 1–426 (1913).
16. Urban, D. J. et al. A new developmental mechanism for the separation of the mammalian middle ear ossicles from the jaw. *Proc. R. Soc. B* **284**, 20162416 (2017).
17. Anthwal, N. et al. Meckel's cartilage breakdown offers clues to mammalian middle ear evolution. *Nature Ecol. Evol.* **1**, (2017).
18. Hylander, W. L. The functional significance of primate mandibular form. *J. Morph.* **160**, 223-239 (1979)
19. Herring, S. W., Rafferty, K. L., Liu, Z. J., & Marshall, C. D. Jaw muscles and the skull in mammals: the biomechanics of mastication. *Comp. Biochem. Phys. A.* **131**, 207-219 (2001).
20. Liu, Z.J. & Herring, S.W. Bone surface strains and internal bony pressures at the jaw joint of the miniature pig during masticatory muscle contraction. *Arch. Oral Bio.* **45**, 95-112 (2000).
21. Crompton, A. W. in *Functional Morphology in Vertebrate Paleontology* (ed J. J. Thomason) 55-75 (Cambridge University Press, 1995).
22. Lautenschlager, S. *et al.* Morphological evolution of the mammalian jaw adductor complex. *Biol. Rev.* **92**, 1910-1940 (2017).
23. Reed, D. A. Iriarte-Diaz, J., Diekwisch, T. G. H. A three dimensional free body analysis describing variation in the musculoskeletal configuration of the cynodont lower jaw. *Evol. Develop.* **18**, 41-53 (2016).

24. Rowe, T. Phylogenetic systematics and the early history of mammals. In *Mammal Phylogeny* (pp. 129-145). Springer New York, (1993).
25. Kemp, T. S. The origin of higher taxa: macroevolutionary processes, and the case of the mammals. *Acta Zool.* **88**, 3-22 (2007).
26. Hanken, J., & Wake, D. B. Miniaturization of body size: organismal consequences and evolutionary significance. *Ann. Rev. Ecol. Syst.* **24**, 501-519 (1993).
27. Gill, P. *et al.* Dietary specializations and diversity in feeding ecology of the earliest stem mammals. *Nature* **512**, 303-307 (2014).
28. Close, R. A., Friedman, M., Lloyd, G. T., & Benson, R. B. Evidence for a mid-Jurassic adaptive radiation in mammals. *Current Biology* **25**, 2137-2142, (2015).
29. Pacheco, C. P., Martinelli, A. G., Pavanatto, A. E., Soares, M. B., & Dias-da-Silva, S. *Prozostrodon brasiliensis*, a probainognathian cynodont from the Late Triassic of Brazil: second record and improvements on its dental anatomy. *Historical Biology* 1-11, (2017).

Acknowledgments We thank P. Brewer, S. Chapman (Natural History Museum, London), O. Rauhut, G. Roessner (Bayerische Staatssammlung fuer Historische Geologie und Palaeontologie, Munich), K. Angielczyk, W. Simpson (Field Museum of Natural History, Chicago), G. Hantke and A. Kitchener (National Museums of Scotland, Edinburgh) for access to specimens in their care. T. Rowe and J. Maisano (University of Texas, Austin) generously provided digital data sets of specimens. A. Neander (University of Chicago), G. Roessner (Bayerische Staatssammlung fuer Historische Geologie und Palaeontologie, Munich), D. Sykes (Natural History Museum London), K. Robson Brown (University of Bristol), O.Katsamenis and M. Mavrogordato (University of Southampton) assisted with CT scanning. J. Hopson (University of Chicago) is thanked for discussion. Three anonymous reviewers are thanked for helpful suggestions improving earlier manuscript versions. This

work was funded by NERC (Natural Environment Research Council) grants NE/K01496X/1 (to E.J.R.) and NE/K013831/1 (to M.J.F.), and support from the University of Chicago (to Z.-X. L).

Author contributions

S.L., P.G., Z.-X. L., M.F and E.R. conceived and designed the study. S.L., P.G., Z.-X. L., and E.R. arranged logistics of specimens for CT scanning and collected CT data. Z.-X. L. provided access to additional specimens and data. S.L. processed CT data, performed digital restorations and reconstructions, performed computational analyses. M.F and E.R. contributed to FEA and MDA analyses. S.L., P.G., Z.-X. L., M.F and E.R equally contributed to the analysis of results. S.L. prepared main text, figures and supplementary data. S.L., P.G., Z.-X. L., M.F and E.R equally contributed to editing, commenting and revising the manuscript and figures. M.F. and E.R. acquired funding.

Competing interests

The authors declare no competing interests.

Corresponding author

Correspondence to Stephan Lautenschlager (s.lautenschlager@bham.ac.uk) or Emily Rayfield (e.rayfield@bristol.ac.uk)

Data availability. All relevant data (three-dimensional osteological, FEA and MDA models, computer code) are made available via the University of Bristol's DataBris repository.

FIGURE CAPTIONS

Figure 1 | Mandibular sizes and evolutionary relationships of cynodonts, mammaliaforms and mammals. Asterisk denotes studied taxa. Phylogeny simplified after Luo et al.[13], Close et al.[28] and Pacheco et al.[29].

Figure 2 | Biomechanical analysis of cynodont and mammaliaform taxa for simulated unilateral biting at canines and most posterior tooth. a-g, MDA plots showing bite forces and joint forces (working and balancing side) during jaw opening and closing cycles. Range bars denote bite force values obtained from the FE models. Peak values in red represent maximum bite force obtained from MDA models. **h-n,** FE von Mises stress contour plots for bite at canine and last tooth (indicated by red arrows). Scale bars for (h, j-n) 10 mm, (i) 50 mm. Sample size for each species n = 1.

Figure 3 | Von Mises stress contour plots of mandibular joint region. a-g, Jaw joint of the working side in dorsal view, **h-n,** jaw joint of the balancing side in dorsal view. All contour plot images scaled to the same size. Results shown for simulated unilateral bite at the most posterior tooth.

Figure 4 | Muscle activation patterns and joint stress calculations a, Muscle activation simulation to achieve highest bite forces relative to minimum tensile and compressive stress at the jaw joint. Muscle combinations for the five highest bite force vs stress outputs shown for all taxa in decreasing order (1-5). Reconstructed adductor muscle groups depicted in skull images. **b,** Tensile and compressive stresses in the jaw joint and percentage reduction (‘loss’) in bite force (relative to largest model of 320mm) of all taxa, each scaled to seven different

292 jaw lengths. Relative bite force reduction is the same for all models with each successive size
293 and represented by a single trend line.
294

METHODS

Specimens and digital models. Three-dimensional digital models of key cynodont and mammaliaform taxa were created for this study using the following specimens: *Thrinaxodon liorhinus* (NHMUK PV R 511, 511a, Natural History Museum, London, UK), *Diademodon tetragonus* (BSP 1934 VIII 17/2, Bayerische Staatssammlung für Historische Geologie und Paläontologie, Munich, Germany), *Probelesodon sanjuanensis* (PVSJ 411, Museo de Ciencias Naturales, Universidad Nacional de San Juan, Argentina), *Probainognathus* sp. (PVSJ 410), *Morganucodon oehleri* (FMNH CUP 2320, Field Museum of Natural History, Chicago, USA; IVPP 8685, Institute for Vertebrate Palaeontology and Palaeoanthropology), *Morganucodon watsoni* (NHMUK PV M 26144, articulated squamosal and petrosal; NHMUK PV M 92838 & M 92843, isolated quadrates; NHMUK PV M 27410, isolated fragmentary jugal), *Hadrocodium wui* (IVPP 8275), *Monodelphis domestica (*National Museum of Scotland, Edinburgh*).* All specimens were digitised using CT scanning or (as in the case of *Diademodon tetragonus*) a photogrammetry approach. For scan details see[21]. For the model creation and the removal of taphonomic artefacts, scan data were imported into Avizo (version 8, VSG, Visualisation Science Group). Data sets were segmented manually in Avizo segmentation editor to separate bone from the surrounding matrix. As all fossil specimens exhibited various preservational and taphonomic artefacts, different restoration steps were applied as outlined in detail in Lautenschlager[22,29]: For a detailed account of the restorative steps of the individual specimens the reader is referred to the supplementary information and Lautenschlager et al.[22].

Three-dimensional models of the jaw adductor muscle anatomy of all fossil specimens were reconstructed digitally following a protocol outlined in Lautenschlager[30]. Reconstructions were performed on the basis of osteological correlates indicating muscle attachment sites. Where exact locations and boundaries between adjacent attachments were

unclear, topological criteria were applied. Corresponding insertions and origins of each muscle were connected by simple point-to-point connections to evaluate the muscle arrangement and to identify possible intersections or other conflicts. Following this initial reconstruction, muscle dimensions and volumes were modelled according to spatial constraints within the bony structure. Data obtained from contrast-enhanced CT scanning of *Monodelphis domestica* was consulted to further inform the fossil muscle reconstructions. Competing hypotheses regarding the exact placement and arrangement of specific muscles were evaluated by analysing muscle strain[22,31]. Full details and discussion of the reconstructed jaw adductor complex across the studied taxa can be found in Lautenschlager et al.[22]. The final muscle reconstructions were used to supply input parameters for the subsequent finite element analysis (FEA) and multibody dynamics analysis (MDA). Muscle forces were calculated based on physiological cross-section area[32], which was estimated by dividing the volume of each muscle by its total length (supplementary table S2).

Multibody dynamics analysis. For MDA, the digitally restored models of all taxa were imported into Adams (version 2013.2, MSC Software Corp.) as rigid bodies in .x_t parasolid format. The skull and jaw models were aligned manually to articulate at the quadrate-articular joint or the squamosal-dentary joint, respectively. Throughout all simulations, the skull models were kept immobile; the jaw models were allowed mobility in all degrees of freedom. Skull and jaw models were connected by spherical joint elements in Adams. Mass and inertial properties were calculated in Adams based on rigid body geometry and an average bone density of 1764 kg/m^3 [33]. The different adductor muscle groups were modelled as a series of spring elements linking corresponding muscle insertion and origin sites. Muscle forces were assigned according to the calculations taken from the three-dimensional reconstructions. Muscle activation was modelled by applying a dynamic geometric

optimisation (DGO) method[34]. Unilateral and bilateral biting at the canines and the posteriormost tooth position were simulated using a rigid body box element from the Adams solids library. The box was placed perpendicular to the teeth at the aforementioned tooth positions and moved posteriorly during jaw opening phases. Bite forces and joint reaction forces for the working and balancing side joints (for the unilateral bite scenarios) were recorded throughout the bite simulations.

Two sets of simulations were performed for each taxon: (i) all models scaled to the actual size of the physical specimens, (ii) all taxa scaled to the same surface area to evaluate the biomechanical effects of morphological differences independent of size[35]. For the latter scenario, the model of *Thrinaxodon liorhinus* was selected as the reference as it represents approximately the average size of all models (which range in jaw length between 13mm and 270mm); all other models were scaled to the same surface area as the *Thrinaxodon* model.

Finite element analysis. For FEA, jaw models of all taxa were imported into Hypermesh (version 11, Altair Engineering) for the creation of solid mesh FE models and the setting of boundary conditions. All jaw models consisted of approximately 2,500,000 tetrahedral elements. Material properties for mandibular bone and teeth were assigned based on nano-indentation results for hedgehog mandibles (bone: E = 12 GPa, υ = 0.30, tooth: E = 25.0 GPa, υ = 0.3); material properties for mammalian mandibular sutures were taken (E = 46.0 MPa, υ = 0.35) from literature data[36]. Due to the resolution of some CT datasets, cortical and cancellous bone were not differentiated, permitting the use of models derived from different digitisation methods (volumetric: computed tomography; surface-based: photogrammetry). All materials were treated as isotropic and homogenous. To avoid artificially high stress and strain peaks on the articular and dentary, constraints were not directly applied to the joint region. Instead, an additional component with the same material properties was created to

articulate with the joint surface. The morphology of these linking components was based on the cranial articulating joint morphology. The linking components were constrained (15 nodes on each side) from translation in x-, y-, and z-direction. To simulate biting at different analogous positions, additional constraints (one node each, in x-, and y- direction, z-direction unrestrained to allow penetration of tooth into prey) were applied to the canine and the posteriormost tooth, each for a unilateral and a bilateral scenario. Muscle forces were assigned according to the calculations taken from the three-dimensional reconstructions (supplementary table S2). As for the MDA, a second set of simulations was performed with all models scaled to the same surface area and muscle forces scaled proportionally to analyse the models at the same relative size[34]. The models were subsequently imported into Abaqus 6.10 (Simulia) for analysis and post-processing. Biomechanical performance of the FE models was assessed via contour plot outputs. In addition, reaction forces (= bite forces) at the bite points and average stress, strain and displacement values per element were obtained from the models.

For the simulation of different muscle activation patterns, load forces for the temporalis, the masseter and the pterygoideus groups were varied: each muscle group was set up to successively produce 0, 25, 50, 75 and 100% of the maximum force and all possible permutations were simulated (resulting in $5^3 = 125$ possible combinations, for the five different states and three muscle groups). To automate this process, an R script was used to modify the FEA input files accordingly[37]. All other settings were kept constant as outlined above and analysed using Abaqus. To compare performances, bite force values and average joint stresses (von Mises, tensile, compressive) were obtained from Abaqus. Average joint stresses were calculated from 30 nodes selected in a grid pattern on the surface of the jaw joint to obtain a maximum spread and analogous point across all taxa. Results of the different

muscle activation simulations were plotted in a three-dimensional coordinate system using the freely-available visualisation package Blender (www.blender.org) (Figs. S7-S12).

Additional FEA simulations were performed for all taxa scaled to different, discrete mandible lengths: 5, 10, 20, 40, 80, 160 and 320mm. Mandible lengths were chosen to represent the range of sizes observed across the cynodont-mammaliaform transition. Load forces were scaled for each size stage following the ¾ power law for each taxon.

29. Lautenschlager, S. Reconstructing the past: methods and techniques for the digital restoration of fossils. *Royal Soc. Open Sci.* **3**, 160342 (2016).
30. Lautenschlager, S. Cranial myology and bite force performance of *Erlikosaurus andrewsi*: A novel approach for digital muscle reconstructions. *J. Anat.* **222**, 260-272 (2013).
31. Lautenschlager, S. Estimating cranial musculoskeletal constraints in theropod dinosaurs. *Royal Soc. Open Sci.* **2**, 150495 (2015).
32. Thomason, J. J. Cranial strength in relation to estimated biting forces in some mammals. *Canad. J. Zool.* **69**, 2326–2333 (1991).
33. Ashman, R. B. & Rho, J. Y. Elastic modulus of trabecular bone material. *J. Biomech.* **21**, 177-181 (1988).
34. Curtis, N. *et al.* Predicting muscle activation patterns from motion and anatomy: modelling the skull of *Sphenodon* (Diapsida: Rhynchocephalia). *J. Royal Soc. Interface* **7**, 153-160 (2010).
35. Dumont, E. R., Grosse, I. R., Slater, G. J. Requirements for comparing the performance of finite element models of biological structures. *Journal of Theoretical Biology* **256,** 96-103 (2009).
36. Bright, J. A. The importance of craniofacial sutures in biomechanical finite element models of the domestic pig. *PLOS one* **7**, e31769 (2012).

37. R Core Team (2017). R: A language and environment for statistical computing. R Foundation for Statistical Computing, Vienna, Austria. URhttps://www.R-project.org/

EXTENDED DATA FIGURES CAPTIONS

Extended data figure 1 | Relative bite forces and biomechanical performance measures of cynodont and mammaliaform taxa. a, Relative bite forces for original sized models. **b,** Relative bite forces for models scaled to the same size (with *Thrinaxodon liorhinus* as reference). Relative bite forces calculated as ratio between muscle forces and resultant bite forces (obtained from reaction forces of FE models). Range of values represents results for unilateral and bilateral bite simulations. Average per element values for **c,** Von Mises stress, **d,** displacement, **e,** maximum principal strain, and **f,** minimum principal strain. Range of values represents results for unilateral and bilateral bite simulations (for original sized models). Sample size for each species n = 1.

Extended data figure 2 | Biomechanical analysis results of cynodont and mammaliaform taxa for simulated unilateral biting at canines and last tooth. Results for models scaled to the same size (with *Thrinaxodon liorhinus* as reference). **a-g,** MDA plots showing bite forces and joint forces (working and balancing side) during jaw opening and closing cycles. Range bars denote values obtained from reaction forces of FE models. Peak values represent maximum bite force obtained from MDA models. **h-n,** FE von Mises stress contour plots for bite at canine and last tooth (indicated by red arrows). Scale bars for (h, j-n) 10 mm, (i) 50 mm. Sample size for each species n = 1.

Extended data figure 3 | Tensile and compressive stress contour plots of mandibular joint region. Results shown for unilateral bite at the canine (upper rows) and the last tooth position (lower rows), each for the jaw joint of the working side and the balancing side in dorsal view. All contour plot images scaled to the same size.

Extended data figure 4 | Bite force magnitude vs von Mises stress for different muscle activation patterns. Results shown for unilateral bite at the canine tooth position. Relative bite force measured as bite force in relation to von Mises stress occurring in the jaw joint.

Extended data figure 5 | Bite force magnitude vs von Mises stress for different muscle activation patterns. Results shown for unilateral bite at the last tooth position. Relative bite force measured as bite force in relation to von Mises stress occurring in the jaw joint.

Extended data figure 6 | Bite force magnitude vs tensile stress for different muscle activation patterns. Results shown for unilateral bite at the canine tooth position. Relative bite force measured as bite force in relation to tensile stress occurring in the jaw joint.

Extended data figure 7 | Bite force magnitude vs tensile stress for different muscle activation patterns. Results shown for unilateral bite at the last tooth position. Relative bite force measured as bite force in relation to tensile stress occurring in the jaw joint.

Extended data figure 8 | Bite force magnitude vs compressive stress for different muscle activation patterns. Results shown for unilateral bite at the canine tooth. Relative bite force measured as bite force in relation to compressive stress occurring in the jaw joint.

Extended data figure 9 | Bite force magnitude vs compressive stress for different muscle activation patterns. Results shown for unilateral bite at the last tooth. Relative bite force measured as bite force in relation to compressive stress occurring in the jaw joint.

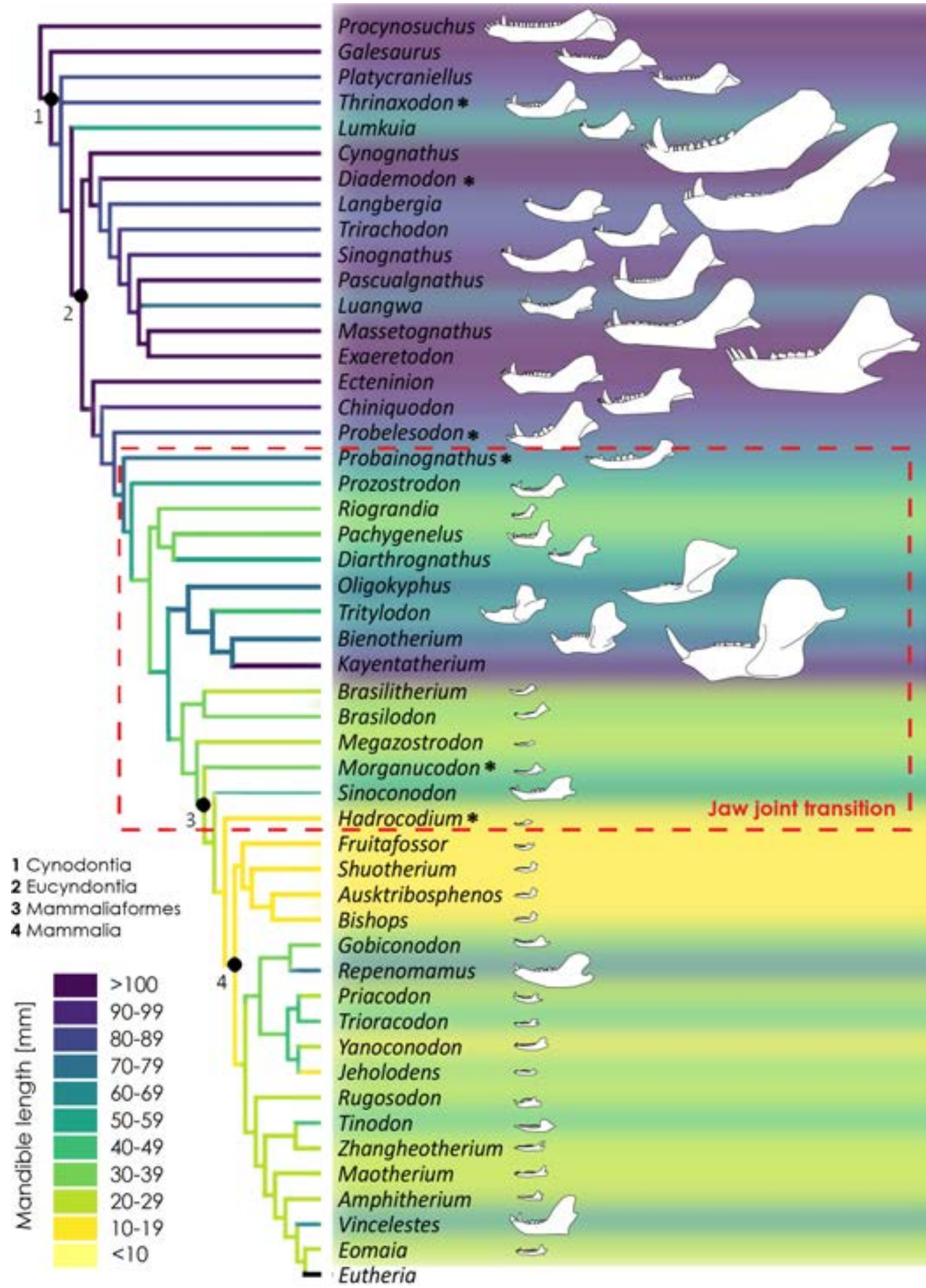
Procynosuchus
Galesaurus
Platycraniellus
Thrinaxodon *
Lumkuia
Cynognathus
Diademodon *
Langbergia
Trirachodon
Sinognathus
Pascualgnathus
Luangwa
Massetognathus
Exaeretodon
Ecteninion
Chiniquodon
Probelesodon *
Probainognathus *
Prozostrodon
Riograndia
Pachygenelus
Diarthrognathus
Oligokyphus
Tritylodon
Bienotherium
Kayentatherium
Brasilitherium
Brasilodon
Megazostrodon
Morganucodon *
Sinoconodon
Hadrocodium *
Jaw joint transition
Fruitafossor
Shuotherium
Ausktribosphenos
Bishops
Gobiconodon
Repenomamus
Priacodon
Trioracodon
Yanoconodon
Jeholodens
Rugosodon
Tinodon
Zhangheotherium
Maotherium
Amphitherium
Vincelestes
Eomaia
Eutheria
1
2
3
4
1 Cynodontia
2 Eucyndontia
3 Mammaliaformes
4 Mammalia
Mandible length [mm]
>100
90-99
80-89
70-79
60-69
50-59
40-49
30-39
20-29
10-19
<10

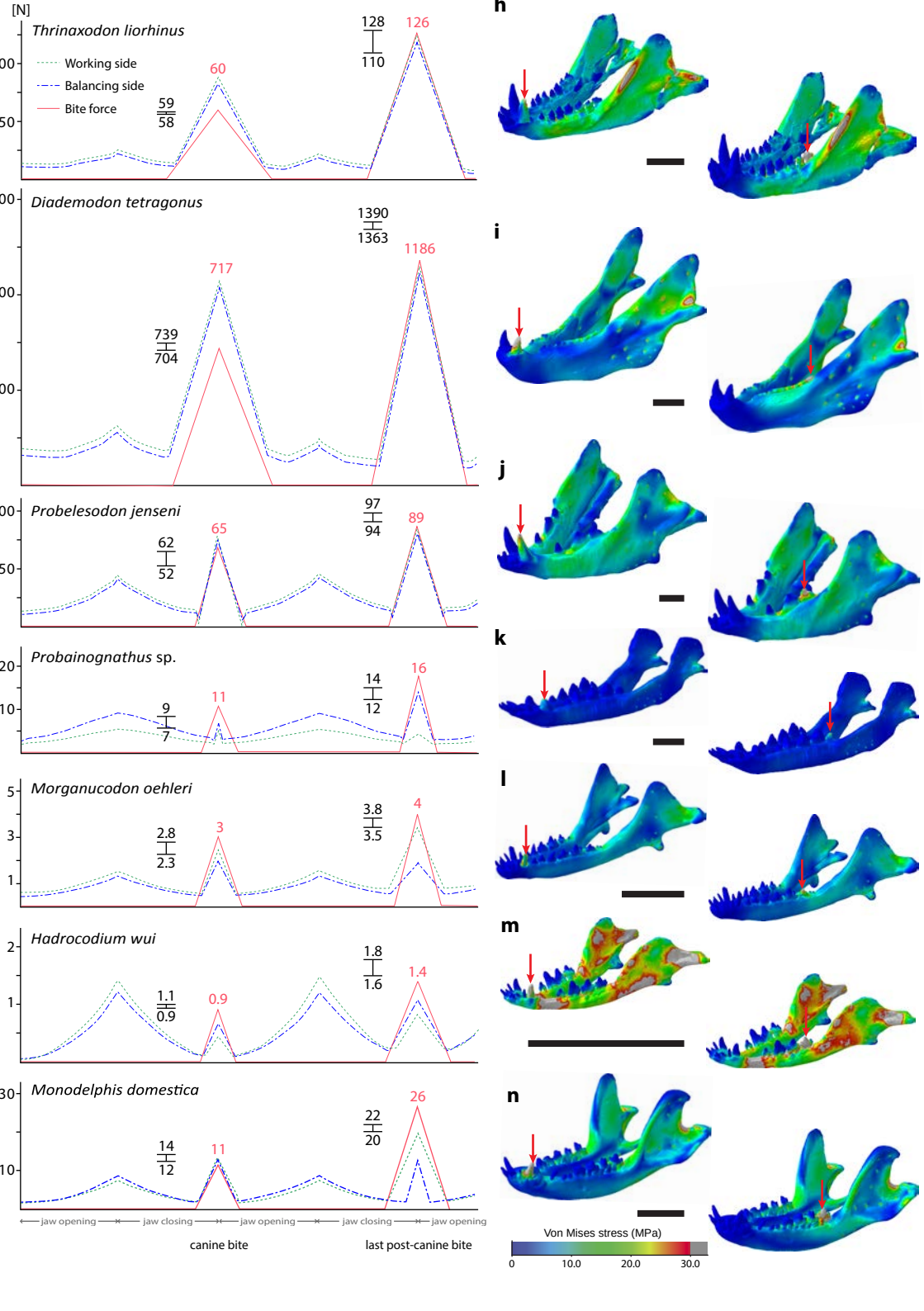
[N]
Thrinaxodon liorhinus
Working side
Balancing side
Bite force
128
110
126
60
59
58
Diademodon tetragonus
1390
1363
1186
717
739
704
Probelesodon jenseni
97
94
89
65
62
52
Probainognathus sp.
14
12
16
11
9
7
Morganucodon oehleri
3.8
3.5
4
3
2.8
2.3
Hadrocodium wui
1.8
1.6
1.4
0.9
1.1
0.9
Monodelphis domestica
22
20
26
11
14
12
jaw opening
jaw closing
jaw opening
jaw closing
jaw opening
canine bite
last post-canine bite
h
i
j
k
l
m
n
Von Mises stress (MPa)
0
10.0
20.0
30.0

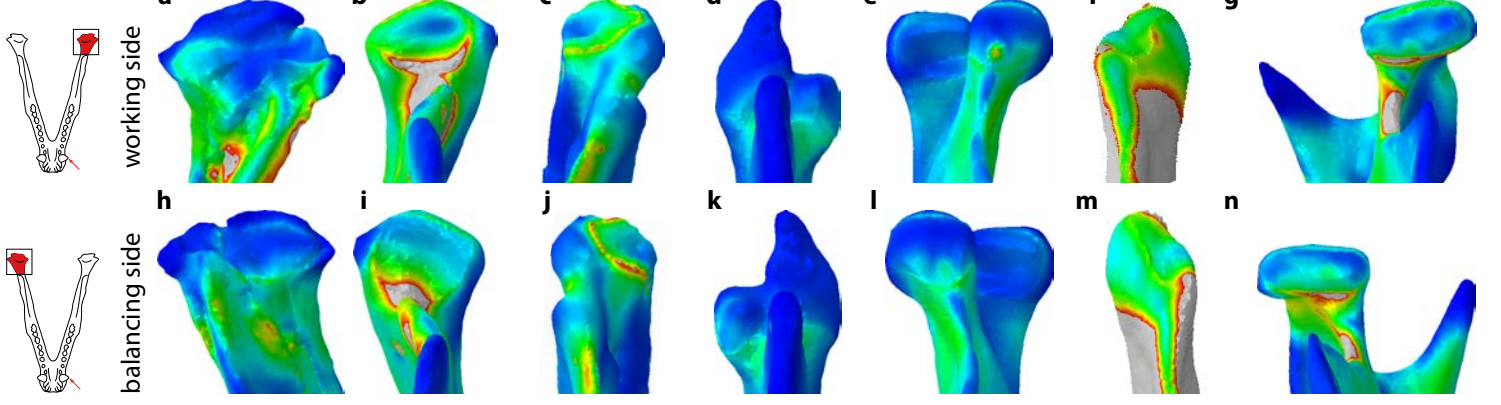
working side
balancing side
a
b
c
d
e
f
g
h
i
j
k
l
m
n
Thrinaxodon
Diademodon
Probelesodon
Probainognathus
Morganucodon
Hadrocodium
Monodelphis
Von Mises stress (MPa)
0
10.0
20.0
30.0

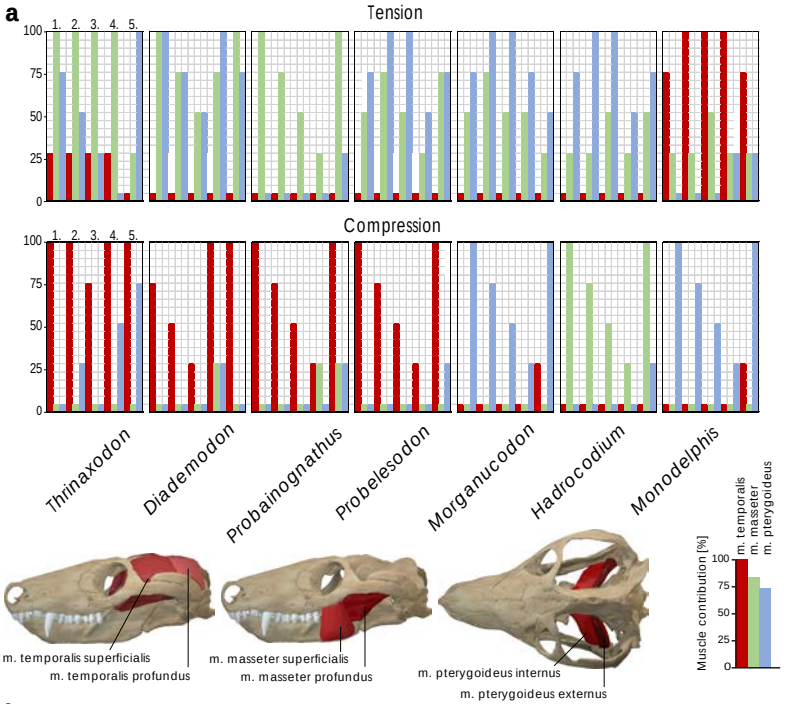
a
Tension
Compression
1. 2. 3. 4. 5.
100
75
50
25
0
Thrinaxodon
Diademodon
Probainognathus
Probelesodon
Morganucodon
Hadrocodium
Monodelphis
m. temporalis superficialis
m. temporalis profundus
m. masseter superficialis
m. masseter profundus
m. pterygoideus internus
m. pterygoideus externus
Muscle contribution [%]
m. temporalis
m. masseter
m. pterygoideus

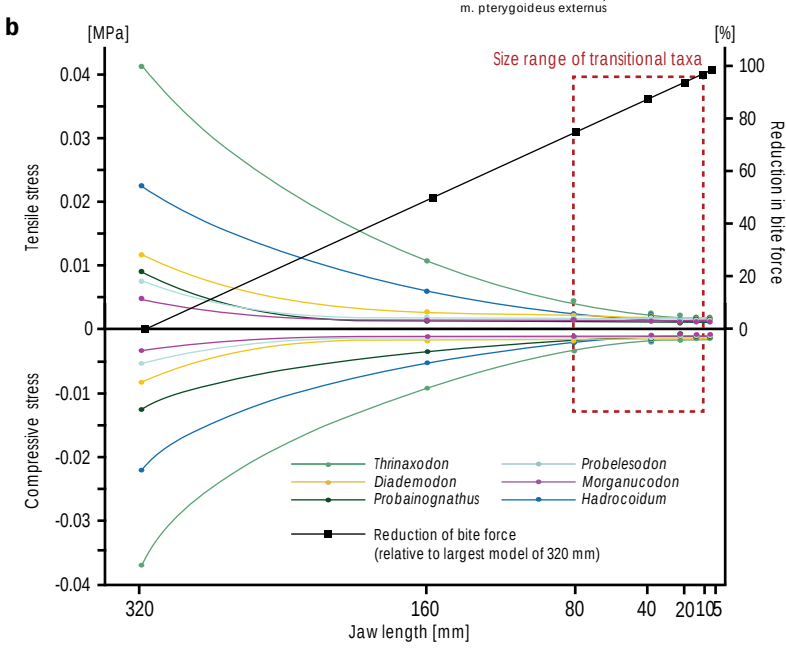
b
[MPa]
[%]
Size range of transitional taxa
Tensile stress
Compressive stress
Reduction in bite force
0.04
0.03
0.02
0.01
0
-0.01
-0.02
-0.03
-0.04
100
80
60
40
20
0
Thrinaxodon
Diademodon
Probainognathus
Probelesodon
Morganucodon
Hadrocoidum
Reduction of bite force
(relative to largest model of 320 mm)
320
160
80
40
20
10
5
Jaw length [mm]